

Article

A Novel Method for Thermal Modelling of Photovoltaic Modules/Cells under Varying Environmental Conditions

Ali Kareem Abdulrazzaq * , Balázs Plesz  and György Bognár 

Department of Electron Devices, Budapest University of Technology and Economics, Hungarian Scientists Tour 2, H-1117 Budapest, Hungary; plesz@eet.bme.hu (B.P.); bognar@eet.bme.hu (G.B.)

* Correspondence: kareem@eet.bme.hu; Tel.: +36-1-463-3073

Received: 12 May 2020; Accepted: 20 June 2020; Published: 29 June 2020



Abstract: Temperature has a significant effect on the photovoltaic module output power and mechanical properties. Measuring the temperature for such a stacked layers structure is impractical to be carried out, especially when we talk about a high number of modules in power plants. This paper introduces a novel thermal model to estimate the temperature of the embedded electronic junction in modules/cells as well as their front and back surface temperatures. The novelty of this paper can be realized through different aspects. First, the model includes a novel coefficient, which we define as the forced convection adjustment coefficient to imitate the module tilt angle effect on the forced convection heat transfer mechanism. Second, the new combination of effective sub-models found in literature producing a unique and reliable method for estimating the temperature of the PV modules/cells by incorporating the new coefficient. In addition, the paper presents a comprehensive review of the existing PV thermal sub-models and the determination expressions of the related parameters, which all have been tested to find the best combination. The heat balance equation has been employed to construct the thermal model. The validation phase shows that the estimation of the module temperature has significantly improved by introducing the novel forced convection adjustment coefficient. Measurements of polycrystalline and amorphous modules have been used to verify the proposed model. Multiple error indication parameters have been used to validate the model and verify it by comparing the obtained results to those reported in recent and most accurate literature.

Keywords: module temperature; solar energy; thermal modelling; heat transfer mechanisms

1. Introduction

The increasing need for electricity and the risks of environmental pollution and global warming are the main problems increasing the interest in renewable and clean energy sources [1]. Solar energy sources using photovoltaic (PV) modules recently have the main focus among other renewable sources. This is due to several reasons such as the abundance of the solar irradiance, the photovoltaic (PV) phenomenon, by which a direct conversion is achieved from solar radiation to electricity, employable at both small and large scale, non-polluting, clean and reliable energy sources. The increase in the temperature of the silicon-based technology PV modules has direct effect on the current–voltage (I–V) characteristics of the device, that is, adversely affecting the power production and causes a significant drop in efficiency [2,3]. Therefore, it is insufficient to rely only on the rated efficiency to estimate the output power. One has to consider the operating temperature of the PV module as well as other environmental conditions and structural parameters [4]. The temperature of the PV module is affected by the module material compositions, mounting structure and the environmental conditions [5,6].

Multiple heat sources are physically contributing to the increment of the module temperature [5]. The first is the incoming short-wave solar irradiance, where only up to 20% will be converted to electrical energy, and the rest will be converted to thermal energy [4,7]. The second heat source is the long-wave infrared radiation. Accurate temperature prediction is not only needed for a precise prediction of the output power, but is also essential for estimating lifetime and quantifying the degradation of PV modules [7–10].

The heat generated in the PV module is conducted through the stacked layers of the PV module to the external surfaces (front and back surface). Radiation, forced convection and free convection heat transfer mechanisms are involved in dissipating the generated thermal energy from the surfaces to the surrounding environment. Therefore, a robust PV thermal modelling is required to estimate the operating temperature of the PV module under the given environmental, physical and structural conditions. These conditions are represented by physical parameters, which act as an input for the model.

The main objective of this work is to propose a novel thermal model to estimate the PV module temperatures at three different planes: The semiconductor p-n junction (electronic junction temperature), the front and the back surface of the PV module. The proposed model is constructed by new combination of effective sub-models found in the literature and including a novel solution for considering the effect of the module tilt angle on the forced convection heat transfer mechanism.

2. Thermal Modelling General Considerations

This section discusses the main environmental, physical and structural parameters that determine the thermal behaviour of a PV module.

2.1. Physical Structures of Pv Modules

An accurate description of the PV module is fundamental to achieve precise estimation for the operating temperature as well as its profile through different layers. Although the photovoltaic technologies are advancing rapidly with higher efficiency and lower cost, the basic solar module physical structure has not changed much over the years [11]. Figure 1 shows the basic structure of a typical PV module.

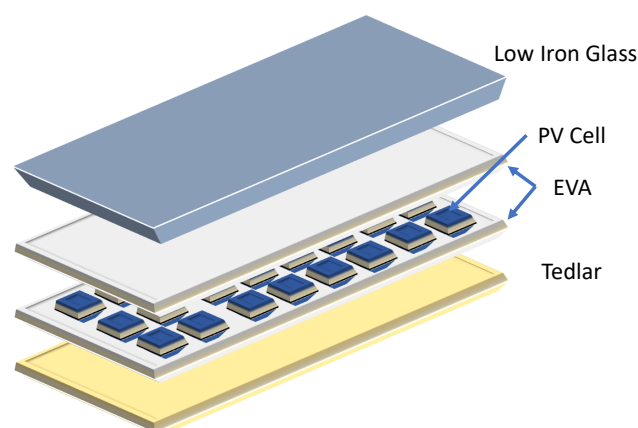


Figure 1. Schematic structure of a basic photovoltaic (PV) module.

The active semiconductor layer is consisting of several photovoltaic cells interconnected in series and parallel depending on the required output current and voltage levels. The active layer is encapsulated between two layers of, as a most often used material, ethylene-vinyl acetate (EVA) to bind the PV cells to the top and bottom layers and provide moisture resistance and electrical insulation [6,12]. Fundamentally, the glass layer is tempered (to increase the mechanical strength of the module), highly transparent, low iron content and has a textured upper-surface (to reduce the solar

irradiance reflection and absorption losses). The back layer is usually made of tedlar polymer that is functioning as irradiance blocker and also providing moisture resistance [13]. Anti-reflection coating (ARC) layer is typically added to the PV layer for efficient light trapping (not shown in Figure 1) [14]. The active semiconductor layer may consist of materials like mono-crystalline, polycrystalline or amorphous silicon.

2.2. Parameters That Affect the Pv Module Thermal Behaviour

A well-known fact is that the temperature has a direct effect on the output power of the PV module. The maximum output power is decreased by 0.3 to 0.5% per Kelvin of temperature increase [15,16]. This is because the open-circuit voltage decreases significantly with increasing temperature while the short-circuit current increases only slightly [17]. However, several parameters affect the PV module temperature. These parameters have a different impact on the temperature value; therefore, some of them are essential to be considered when constructing the thermal model. Following is a list of these parameters [4,5,13,18–23].

- The amount of solar irradiance captured by the module and its spectral distribution.
- Ambient temperature.
- Wind speed, direction and air flow pattern.
- Relative humidity.
- The PV module electrical conversion efficiency.
- The PV module materials optical and thermal parameters such as irradiance absorptivity, thermal conductivity, etc.
- Mounting structure of the PV module.
- Homogeneity of the irradiance over the module surface.
- The connected electrical load.
- PV technology.

Some of these parameters are strongly influencing the module temperature; however, other parameters effect the thermal properties of the module only to a smaller extent [24]. For example, the module temperature is highly sensitive to the wind speed and much less to the wind direction [25,26]. Some of these parameters are not easy to be included in a general approach for estimating the module temperature since the module thermal behaviour is changing for different technologies [17].

3. Thermal Modelling Concepts

This section will review different thermal modelling techniques and focuses mainly on the energy balance and heat transfer mechanisms.

3.1. Classification of Pv Modules Thermal Modelling Concepts

The wide range of parameters that affect the PV module temperature (material and environmental parameters) as well as different heat transfer mechanisms that take place through the module or on its surfaces give rise to the need of complex models for estimating the junction temperature. However, for commercial products, the manufacturers do not provide all of the required information. Generally speaking, the module temperature is a dynamic, nonlinear and implicit function incorporating the controlling parameters [9]. Factors like the required level of the accuracy, details of the temperature changing profile and the model complexity produce different types of modelling approaches. Many researchers treated temperature variation as a static function; hence, it is abruptly changing to reach a steady state. That is, neglecting the material thermal capacity effect and discarding the lag in temperature variation with respect to one or more of the affecting parameters [6]. Based on this concept, the main classification of the PV temperature modelling is whether it is a static

(steady-state) [12,15–17,22,25,27,28] or dynamic model [2,5–7,18,29–33]. Although the static model requires lower computational cost, its accuracy level could be affected in case of rapid changing of the controlling parameters. Temperature requires time between 4 and 10 minutes to reach the steady-state from its initial value, depending on the difference between the initial and the final temperatures and the PV module technology [5,34]. When the model input parameters are available with a frequency below this range, the dynamic model will be applicable for an accurate evaluation of the temperature [12].

The various existing thermal models in the literature, which are different in accuracy and complexity, can be grouped depending on their nature to be represented by the following.

- Direct physical equations based on theoretical expressions to incorporate different environmental, physical and structural parameters [12,15–17]. To create such an explicit relation, physical assumptions and mathematical approximations have to be made.
- Empirical expressions which are mainly based on observations and experimental measurements [25,27,28,35–37]. However, these models are optimised to represent the behaviour of the system under observation and difficult to be generalised to describe other systems, which are based on different technologies. Although these types of models require a low number of input parameters, their output accuracy is questionable [15,38]. Empirical approaches are also used to evaluate the heat transfer mechanisms to be substituted in models that have been constructed using different approaches [5,8,18,31].
- Dimensional analysis of the PV module [4,6,23,34,39]. This type of modelling will provide the capability to investigate the temperature profile and its changing rate through the PV module structure, including different thermal loss mechanisms as boundary conditions. However, it requires relatively high computational cost.
- Evaluating the heat balance equation for each structural layer of the PV module [18,40]. Different layers temperatures are estimated by substituting the effect of various heat transfer mechanisms, including thermal conduction between these layers.
- Treating the PV module as a single block of material and employ a single heat balance equation, including different heat loss mechanisms [2,3,5,7,8,13,19,22,29–33,41,42]. The thermal resistivity and thermal capacity (in case of a dynamic model) will be summed to find the component of the heat generated inside the module. Therefore, the model results will provide the module temperatures, but typically, without details about the temperature profile. The heat balance equation will be used as the core of the model, incorporating different heat loss mechanisms from the module surfaces.

The latter approach, recently, attracts the researchers focus and interest because of its applicability and high level of accuracy for estimating the module temperature. However, different researchers consider different methodologies when building up their thermal models. Based on this approach, this paper aims to propose a new thermal model. Sections 3.2 and 4 will discuss its physical translation and review the existing methods in the literature, respectively.

3.2. Energy Balance and Heat Transfer Mechanisms

It is a well-known fact that electronic junction temperature is not accessible from outside and cannot be directly measured using normal methods. Instead, models are used to estimate its value. One of the widely used methods considers the PV module as a single block of material and employ a single thermal heat balance equation (HBE), in which the absorbed energy ($q_{absorbed}$) should equal to the sum of the converted ($q_{converted}$) and the lost (q_{lost}) energies.

$$q_{absorbed} = q_{converted} + q_{lost} \quad (1)$$

The absorbed energy results from collecting the irradiance by the front surface of the PV module represent the overall input energy for the PV system. The converted energy includes the output

produced electrical energy and the heat energy generated within the PV module. The last term in Equation (1) is related to the heat losses to the surrounding environment by different heat transfer mechanisms. The heat losses can be classified in two groups. The first group is mainly driven by the temperature difference between the module and its surrounding environment. The second group involves different effects such as joule heat in the wire contacts, diode losses and dirt accumulation. Considering all types of heat loss mechanisms gives rise to a complex modelling design that requires various parameters, which are related to the material properties and also the surrounding environment. Such a detailed model is impractical to be used for commercial products. Therefore, some of these losses are neglected due to their minor effects [9]. These minor losses include the energy initiated due to partial shading, low irradiance, dirt accumulation, joule heat through the wire contacts and diodes losses. Conduction heat transfer between the PV module and the holding structure is also neglected because of the small contact area and relatively small temperature difference [3,13,41].

Each of the heat balance equation terms (including their different components) need to be modelled to estimate their values individually because their effects cannot be directly measured [7,29]. Such an analysis should be based on the instantaneous temperature of the PV module. Therefore, an iterative process is needed. Conduction (between the PV module layers), convection and radiation (from front and back surfaces) are the three main heat transfer mechanisms that have to be evaluated to calculate the amount of losses.

Even in case it is not explicitly mentioned, the majority of the existing models share common assumptions, which are listed as follows [3,4,6–9,18,22,31,34,41].

- The temperature has a homogeneous distribution over the surface of the PV module.
- The ground temperature is equal to the ambient temperature.
- The thermal losses from the side edges of the PV module are negligible due to its small area compared to the front and back surfaces.
- The effect of the ARC layer is neglected due to its small thickness compared to other physical layers.
- The effect of the metallic frame that surrounds the PV module structural layer is neglected.
- Each of the PV module physical layers is treated as isothermal, that is, neglecting the boundary effects.
- The optical and physical parameters of the PV module different layers materials are homogeneous, isotropic and not changing with temperature nor the irradiance wavelength.
- The ambient temperature is homogeneous all around the PV module.
- The solar irradiance is reaching the front surface of the PV module equally.
- Neglecting the conduction heat transfer between the PV module and the holding structure.
- Neglecting energy losses due to partial shading, low irradiance, dirt accumulation, joule heat through the wire contacts and diodes losses.

Some researchers are going further in simplifying their models by eliminating other effects or parameters as a result of dealing with specific environmental conditions, materials properties or mounting structures. Table 1 shows some of these simplifications and assumptions.

Table 1. Special case assumptions found in the literature.

#	Introduced Simplifications	Ref.
1	Neglecting the radiation heat losses from the back surface based on the assumption that the back surface of the module is at same temperature of the building fabric it faces.	[29]
2	Back surface emissivity assumed to be equal to the front surface emissivity.	[8]
3	The heat transfer by free convection is assumed to be the same for both top and bottom surfaces. This assumption is applicable for a near vertical angles but introduces error for PV modules mounted flat.	[8]
4	The cell temperature is assumed to be the same as the front surface temperature and it is linearly related to the back surface temperature.	[5]
5	Neglecting the radiation heat losses of both surfaces.	[5,15,33]

Table 1. Cont.

#	Introduced Simplifications	Ref.
6	The total value of convective heat losses is the total of forced convection loss from only the PV module front surface and free convection loss from only the back surface.	[33]
7	The temperature is assumed uniform throughout the PV module five layers.	[13,15]
8	To avoid disturbing influences of fast irradiance changes at sunrise and sunset, the authors only analysed data from 10 am to 3 pm.	[17]
9	Neglecting the forced convection from the back surface.	[39]

4. Reviewing the Existing Sub-Models

As previously mentioned, each of the HBE terms (including their different components) need to be modelled and individually estimated. This section is dedicated to briefly discussing each term of the HBE with scanning the literature to review the typical methods adopted to estimate their values.

4.1. Absorbed Energy

The absorbed energy represents the amount of energy received by the PV module due to the total captured short wave irradiance. Different parameters are affecting the amount of absorbed energy, such as [2,4,6,7] the following.

- The intensity of the direct and the diffused irradiances.
- Optical parameters including the absorptivity, the reflectivity, the scattering and the transmittance of the front layers.
- Material defects and physical limitations.
- Mounting structure of the PV module.

A widely used equation to determine the short wave absorbed energy given as [2,3,29–33]

$$q_{absorbed} = \alpha \cdot \Phi \cdot A, \quad (2)$$

where α is the absorptivity of the front surface of the PV module, Φ is the total received irradiance and A is the surface area.

4.2. Converted Energy

The energy is converted into two forms: electrical energy (q_{elec}) and thermal energy (q_{therm}).

$$q_{converted} = q_{therm} + q_{elec}. \quad (3)$$

To determine the amount of produced electrical energy, the values of the current and voltage at the maximum power point (I_m, V_m) are required. Therefore, the fill factor (FF) and the efficiency of the PV module (η) play a major role as shown below [3,13],

$$q_{elec} = I_m V_m = (FF) I_{sc} V_{oc} = \eta \tau q_{absorbed}, \quad (4)$$

where τ is the front layer transmittance, and I_{sc} and V_{oc} are the short-circuit current and open-circuit voltage, respectively. Many authors, for the sake of a higher level of accuracy, tend to consider the environmental effects on the electrical performance of the PV module. Therefore, they include a dedicated electrical model for estimating the instantaneous value of the generated electric power [19,40]. These details are out of the scope of this paper.

The portion of the absorbed energy not converted to electrical energy is converted to heat, causing higher PV module temperature. With time, the thermal energy will be lost to the surrounding environment, mainly due to the temperature difference. However, this process requires some time before reaching a steady-state depending on the thermal properties of the PV module, represented

by its thermal capacity and resistivity. In case of temperature evaluation is required within small periods, as described in Section 3.1, then the dynamic analysis is required to include different layers' thermal capacity. The module heat capacity (C_{module}) is determined as the sum of each layer's capacity [2,13,29–31] from the following formula,

$$C_{module} = \sum_{i=1}^n A \cdot d_i \cdot \rho_i \cdot c_i, \quad (5)$$

where n is the number of PV module physical layers and i is the layer index. Moreover, in Equation (5) we see, for each layer, A is the area, d is the layer thickness, ρ is the material density and c is the specific heat.

Another modelling approach adopts the concept of assuming that the temperature is abruptly following the changes in the absorbed energy. These methods are applicable in case the module temperature and its output power is required to be estimated with time resolution large enough to reach a steady thermal state, higher than its thermal time constant.

4.3. Heat Transfer Mechanisms

As indicated previously, different heat transfer mechanisms are involved in this context, including conduction (within the PV module), radiation and convection. The rest of this section presents a brief description of each one of these mechanisms.

4.3.1. Conduction Heat Transfer Mechanism

Typically, conduction is only considered between the structural layers of the PV module. Conduction to the holding structure is neglected due to the small contact area between the module and the holding structure and the low-temperature difference. The conduction heat transfer between the different layers is analysed based on the thermal resistivity and the thermal capacity of each layer of the PV module [9]. In such models, the HBE is derived for each layer [18].

4.3.2. Convection Heat Transfer Mechanism

Convection is a heat transfer mechanism between the surfaces of the PV module and the surrounding air based on Newton's law of cooling [43]. It is modelled by the corresponding heat transfer coefficients (h_c). The amount of heat convection per unit area (q_{conv}) is evaluated using the following equation:

$$q_{conv} = -h_c \cdot A \cdot (T_{module} - T_{ambient}), \quad (6)$$

where T_{module} and $T_{ambient}$ are module and ambient temperatures, respectively. The convection heat transfer involves two mechanisms—the forced convection mechanism and the free convection mechanism—which are characterised by forced convection coefficient ($h_{c,forced}$) and the free convection coefficient ($h_{c,free}$), respectively. Different researchers deal with their overall effect to be substituted in Equation (6) in different ways, as shown in Table 2.

Table 2. Determining the overall convection coefficient.

#	Used Expression	Eq. #	Ref.
1	$h_c = h_{c,forced} + h_{c,free}$	T 1.1	[3,29,32]
2	$h_c^3 = h_{c,forced}^3 + h_{c,free}^3$	T 1.2	[5,13,19,22,30]

The significance of both types of convection is differs under different environmental conditions [5,30]. The authors of [33] considered only forced convection for the front surface of the PV module and only free convection for the back surface. Other authors consider only free convection for both surfaces [42]. However, most of the recent literature work that aims for high accuracy is

incorporating both free and forced mechanisms [2,6,31]. Modelling and estimating the value of each of the heat transfer coefficients is performed using various techniques [2,6]. Tables 3 and 4 summarise the well-known equations for estimating the free and forced convection, respectively. The following points are common between the different expressions listed in both tables. If any sub-model in the mentioned table use a different expression or parameter definition it will be explicitly mentioned.

- The module characteristics length (L_c) is taken as the longest dimension.
- ΔT is the temperature difference between the PV module surface and the ambient temperatures.
- β is the air thermal expansion coefficient, which is determined as $\beta = 1/T_f$. T_f is the average between the surface and the ambient temperatures, it is also known as the film temperature.
- Considering that the front and back temperatures are different, the film temperature and the thermal expansion coefficient are different for the two surfaces.
- The Grashof number (Gr) is determined as $Gr = \frac{g \cdot \rho_{air}^2 \cdot \cos(\theta) \cdot \beta \cdot \Delta T \cdot L_c^3}{\mu_{air}^2}$, where g is the acceleration due to Earth's gravity, ρ_{air} is the air density, μ_{air} is the dynamic viscosity of air and θ is the angle of the module to the vertical direction.
- Gr_c is the critical Grashof number at which the Nusselt number starts deviating from laminar behaviour [5].
- Pr is the Prandtl number calculated as $Pr = \frac{c_{p,air} \mu_{air}}{k_{air}}$, where $c_{p,air}$ is the specific heat at constant pressure of air and k_{air} is the air thermal conductivity.
- Ra is the Rayleigh number calculated as $Ra = Gr \cdot Pr$.
- Nu_{free} and Nu_{forced} are the Nusselt number of the free and forced convections, respectively. They are determined explicitly in each model.
- $h_{c,free} = \frac{Nu_{free} \cdot k_{air}}{L_c}$, $h_{c,forced} = \frac{Nu_{forced} \cdot k_{air}}{L_c}$.
- Re is the Reynolds number, defined as $Re = \frac{\rho_{air} L_c}{\mu_{air}} v_w$, where v_w is the wind velocity.

Table 3. Free convection equations.

#	Used Expression	Eq. #	Ref.
1	$h_{c,free} = 1.31 \cdot (T_{module} - T_{ambient})^{\frac{1}{3}}$	T 2.1	[29,32]
2	$Nu_{free} = M \cdot Ra^n$, where M and n are constants depend on the geometry of the surface.	T2.2	[42]
3	$Nu_{free} = 0.68 + 0.67 \cdot (Ra_L \cdot R)^{0.25}$, where R is a function tabulated as $R = [1 + (\frac{0.495}{Pr})^{\frac{9}{16}}]^{\frac{-16}{9}}$. The characteristics length for this model is calculated as $L_c = \frac{A}{2 \cdot (H+W)}$, where A , H and W are the module area, length and width, respectively.	T 2.3	[7,8,30,31]
4	$Nu_{free-f} = 0.13 \cdot (GrPr)^{1/3} - (Gr_cPr)^{1/3} + 0.56 \cdot (Gr_cPr \cdot \cos\theta)^{1/4}$, for $\theta < 60^\circ$	T 2.4a	[22]
	$Nu_{free-f} = 0.13 \cdot Ra^{1/3}$, for $\theta \geq 60^\circ$	T 2.4b	
	$Nu_{free-b} = 0.56 \cdot (Ra \cdot \cos\theta)^{1/4}$, for $\theta < 88^\circ$	T 2.4c	
	$Nu_{free-b} = 0.58 \cdot Ra^{1/5}$, for $88^\circ \leq \theta \leq 90^\circ$ where Nu_{free-f} and Nu_{free-b} are the free convection Nusselt numbers for the front and the back surfaces, respectively. In this model the characteristics length is considered as the module dimension in the direction of the natural air flow. In case wind direction is irrelevant, the authors use the following form $L_c = 4 \cdot A/S$, where S is the perimeter.	T 2.4d	
5	$Nu_{free-f} = [0.825 + \frac{0.387Ra^{1/6}}{[1+(0.492/Pr)^{9/16}]^{8/27}}]^2$	T 2.5a	[2,5]
	$Nu_{free-b} = 0.14[(GrPr)^{1/3} - (Gr_cPr)^{1/3}] + 0.56(Gr_cPr \cos\theta)^{1/4}$ In this model the characteristics length is considered as the module dimension in the direction of the natural air flow.	T 2.5b	
6	$Nu_{free} = 0.825 + \frac{0.387Ra^{1/6}}{[1+(0.492/Pr)^{9/16}]^{8/27}}$, for $Ra > 10^9$	T 2.6a	[3]
	$Nu_{free} = 0.68 + \frac{0.67(\cos\theta)Ra^{1/4}}{[1+(0.492/Pr)^{9/16}]^{4/9}}$, for $Ra \leq 10^9$	T 2.6b	

Table 4. Forced convection equations.

#	Used Expression	Eq. #	Ref.
1	The authors chose $h_{c,forced}$ to be $2 \text{ Wm}^{-2}\text{K}^{-1}$ as a constant value.	T 3.1	[29]
2	$cp_{air} \cdot \rho_{air} = 1300.37 - 456,864 \cdot T_f + 0.0116391 \cdot T_f^2$	T 3.2a	[8]
	$h_{c,forced} = \frac{cp_{air} \cdot \rho_{air} \cdot 0.931 \cdot (\frac{v_w \cdot v_w}{L_c})^{0.5}}{Pr^{\frac{2}{3}}}$	T 3.2b	
	where $cp_{air} \cdot \rho_{air}$ is the specific heat and density product that found by curve fitting. The heat transfer coefficient is assumed to be the same from both surfaces; therefore, the overall coefficient will equal to the value determined in the above equation multiplied by 2.	T 3.2c	
3	$h_{c,forced} = 3.83 \cdot v_w^{0.5} \cdot L^{-0.5}$, for $L_c/L \geq 0.95$	T 3.3a	[22,44]
	$h_{c,forced} = 5.74 \cdot v_w^{0.8} \cdot L^{-0.2}$, for $L_c \ll L$	T 3.3b	
	$h_{c,forced} = 5.74 \cdot v_w^{0.8} \cdot L^{-0.2} - 16.46 \cdot L^{-0.1}$, for $L_c/L < 0.95$ where L is the normal length of the PV module and the characteristics length in this model is determined as $L_c = Rec \cdot v/v_w$.	T 3.3c	
4	$h_{c,forced} = \frac{0.931 \rho_{air} v_w C_p Re^{1/2}}{L_c Pr^{2/3}}$.	T 3.4	[2,30,31]
5	$h_{c,forced} = 5.6212 + 3.9252v_w$, for $v_w < 4.88 \text{ m/s}$.	T 3.5a	[32]
	$h_{c,forced} = (3.290v_w)^{0.78}$, for $4.88 \leq v_w < 30.48 \text{ m/s}$.	T 3.5b	
6	$h_{c,forced} = 8.55 + 2.56v_w$.	T 3.6	[33]
7	$h_{c,forced} = 2.8 + 3.0v_w$.	T 3.7	[40]
8	$h_{c,forced} = \frac{k_{air}}{L_c} (2 + 0.41Re^{0.55})$.	T 3.8	[13]
9	$h_{c,forced} = 2 \frac{k_{air}}{L_c} \frac{0.3387Pr^{1/3}Re^{1/2}}{(1+(0.0468/Pr)^{2/3})^{(1/4)}}$, for $Re \leq 5 \cdot 10^5$.	T 3.9a	[3]
	$h_{c,forced} = 2 \frac{k_{air}}{L_c} Pr^{1/3} (0.037Re^{4/5} - 871)$, for $Re > 5 \cdot 10^5$.	T 3.9b	

4.3.3. Radiation Heat Transfer Mechanism

The heat exchange by radiation heat transfer mechanism involves the long-wave irradiance [9]. The amount of radiative energy per unit time per unit area (q_{rad}) is determined based on the Stefan–Boltzmann law as follows

$$q_{rad} = \epsilon \cdot F \cdot \sigma \cdot (T_{ob}^4 - T_{sur}^4), \quad (7)$$

where σ is the Stefan–Boltzmann constant, T_{ob} is the radiating object temperature, T_{sur} is the surrounding temperature, ϵ is the emissivity of a surface and F is the view factor. Table 5 summarises various existing methods from the literature for estimating the amount of thermal radiation. The following notes are common between the expression listed in Table 5 unless explicitly defined again: If any sub-model in Table 5 uses a different expression or parameter definition it will be explicitly mentioned.

1. The subscript *ground* refers to ground, earth or roof in the reference.
2. The subscript *sky* refers to sky.
3. The subscripts *fs* and *bs* refer to the PV module front surface and back surface, respectively.
4. The subscript *rad-front* refers to the radiation from the front surface of the PV module.
5. The subscript *rad-back* refers to the radiation from the back surface of the PV module.
6. The subscript *mfsky* refers to module front to sky.
7. The subscript *mfgr* refers to module front to ground.
8. The subscript *mbsky* refers to module back to sky.
9. The subscript *mbgr* refers to module back to ground.
10. $F_{mfsky} = \frac{(1+\cos(\beta_{surface}))}{2}$, $F_{mfgr} = \frac{(1-\cos(\beta_{surface}))}{2}$, $F_{mbsky} = \frac{(1+\cos(\pi-\beta_{surface}))}{2}$, $F_{mbgr} = \frac{(1-\cos(\pi-\beta_{surface}))}{2}$, where $\beta_{surface}$ is the tilt angle between the module and the ground.

11. The ground temperature (T_{ground}) is assumed to be equal to the ambient temperature ($T_{ambient}$).
12. Some authors define the radiative heat transfer coefficient (h_{rad}) as: $h_{rad} = \sigma \cdot F_{xy} \cdot \epsilon_x \cdot (T_x^2 + T_y^2)(T_x + T_y)$; therefore, the heat energy per unit time per unit area is $q_{rad} = h_{rad}(T_x - T_y)$

Table 5. Radiation thermal energy losses equations.

#	Used Expression	Eq. #	Ref.
1	$q_{rad} = \sigma(F_{mfsky} \cdot \epsilon_{sky} \cdot T_{sky}^4 + F_{mfgr} \cdot \epsilon_{ground} \cdot T_{ground}^4 - \epsilon_{module} \cdot T_{module}^4)$ <p>In this model, the temperature of the module back surface is assumed to be very close to the building roof where the module is installed. Thus, the heat radiation exchange between the module back surface and both sky and ground are neglected.</p> <p>$T_{sky} = (T_{ambien} - \delta T)$ for clear sky condition where $\delta T = 20K$, $T_{sky} = T_{ambient}$ for overcast condition.</p> <p>$\epsilon_{sky} = 0.95$ for clear conditions; 1.0 for overcast condition, $\epsilon_{ground} = 0.95$, $\epsilon_{module} = 0.9$.</p>	T 4.1	[29]
2	$q_{rad-front} = \sigma \cdot F_{mfsky} \cdot \epsilon_{front} \cdot (T_{fs}^4 - T_{sky}^4) + \sigma \cdot F_{mfgr} \cdot \epsilon_{front} \cdot (T_{fs}^4 - T_{ground}^4)$ $q_{rad-back} = \sigma \cdot F_{mbsky} \cdot \epsilon_{back} \cdot (T_{bs}^4 - T_{sky}^4) + \sigma \cdot F_{mbgr} \cdot \epsilon_{back} \cdot (T_{bs}^4 - T_{ground}^4)$ $T_{sky} = (\epsilon_{sky} \cdot T_{ambien}^4)^{0.25}$ <p>$\epsilon_{sky} = 0.727 + 0.0060 \cdot T_{dew-c}$ during daytime; $0.741 + 0.0062 \cdot T_{dew-c}$ during nighttime, where T_{dew-c} is the dew point temperature measured in degree Celsius.</p> <p>The emissivity of front side (ϵ_{front}) is between 0.9 and 1.</p> <p>The emissivity of the back surface (ϵ_{back}) is assumed to be equal to the front glass emissivity.</p>	T 4.2a T 4.2b	[8]
3	$h_{rad-front} = \sigma \epsilon_{front} [F_{mfsky} \cdot (T_{fs}^2 + T_{sky}^2) \cdot (T_{fs} + T_{sky}) + F_{mfgr} \cdot (T_{fs}^2 + T_{ground}^2) \cdot (T_{fs} + T_{ground})]$ $h_{rad-back} = \sigma \epsilon_{back} [F_{mbsky} \cdot (T_{bs}^2 + T_{sky}^2) \cdot (T_{bs} + T_{sky}) + F_{mbgr} \cdot (T_{bs}^2 + T_{ground}^2) \cdot (T_{bs} + T_{ground})]$ $T_{sky} = 0.0552 \cdot T_{ambien}^{1.5}$ <p>$\epsilon_{front} = 0.85$, $\epsilon_{back} = 0.91$.</p>	T 4.3a T 4.3b	[22]
4	$q_{rad-front} = \sigma \cdot F_{mfsky} \cdot \epsilon_{front} \cdot (T_{fs}^4 - T_{sky}^4) + \sigma \cdot F_{mfgr} \cdot \epsilon_{front} \cdot (T_{fs}^4 - T_{roof}^4)$ $q_{rad-back} = \sigma \cdot F_{mbgr} \cdot \epsilon_{back} \cdot (T_{bs}^4 - T_{rack}^4)$ <p>$T_{sky} = (T_{ambien} - \delta T)$ for clear sky condition in which $\delta T = 20K$, $T_{sky} = T_{ambient}$ for overcast condition.</p> <p>ϵ_{front} and ϵ_{back} is between 0.9 and 1.</p> <p>$F_{mbgr} = 1$, $F_{mbsky} = 0$.</p> <p>The rack temperature T_{rack} is approximated to be equal to the ambient temperature.</p> <p>The roof temperature T_{roof} is calculated as $T_{roof} = T_{ambient} + \alpha_r \Phi_h$, where α_r is the roof absorptivity coefficient and Φ_h is the incoming total solar irradiance on the horizontal plane.</p>	T 4.4a T 4.4b	[30]
5	<p>Same Equations T 4.2a and T 4.2b</p> <p>$\epsilon_{front} = 0.91$, $\epsilon_{back} = 0.85$.</p> $T_{sky} = 0.037536 \cdot T_{ambien}^{1.5} + 0.32 \cdot T_{ambien}$		[3]

5. Detailed Construction of Thermal Model

Constructing the thermal model in this research work is based on the approach of treating the PV module as a single block of material and employing the HBE, including different heat transfer mechanisms. Figure 2 shows the thermal behaviour of a PV module that described by the HBE.

The model will provide the PV module junction temperature as well as the temperature difference to both surfaces. Therefore, both front and back surface temperatures will be estimated. This result will be useful in the validation phase because then we can compare the back surface estimated temperature to the measured one by a thermometer attached to the backside of the PV module. The model was constructed based on different, already existing models from the literature (see Section 4). However, the new model was constructed by incorporating sub-models of different existing models in a new and unique way to yield a new model with improved accuracy. For this, different sub-models of the above

described models were combined and tested, and the combination with the best accuracy was chosen as the mode for this paper. The total absorbed energy is consisting of two components and given as

$$q_{absorbed} = q_1 + q_2, \tag{8}$$

$$q_1 = \alpha_{fg} \cdot A \cdot \Phi, \tag{9}$$

$$q_2 = \tau_{fg} \cdot \alpha_{PV} \cdot A \cdot \Phi \cdot (1 - \eta), \tag{10}$$

where q_1 is the rate of thermal energy absorbed by the tempered glass layer, q_2 is the energy absorbed by the semiconductor layer, τ_{fg} is the transmittance of the glass layer, α_{fg} and α_{PV} is the absorptivity of the front glass and semiconductor layers, respectively.

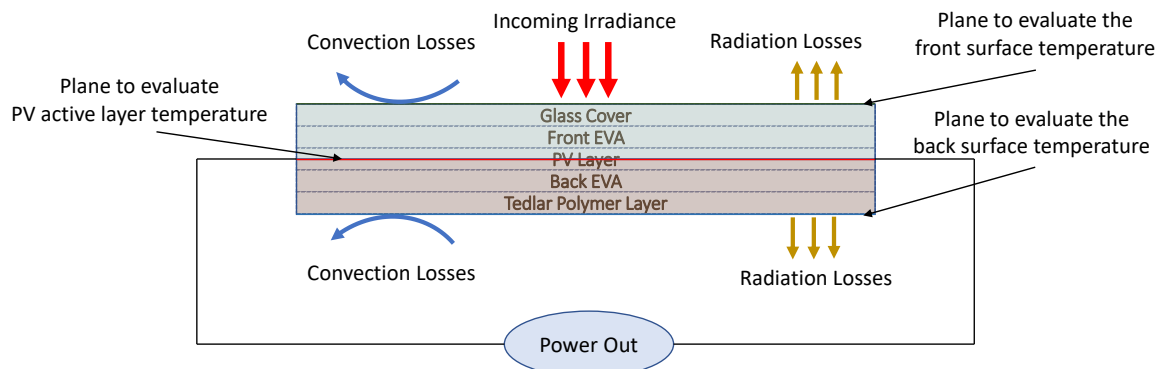


Figure 2. Thermal condition of the PV module.

In this paper, we consider a static model, that is, we assume that the module output power predicted by the proposed model is required only with a time resolution that enables the the temperature to reach a steady state. Therefore, the HBE component which is related to the material thermal capacity is neglected and the converted energy is limited only to the electrical produced component, which is given as

$$q_{converted} = \tau_{fg} \cdot \alpha_{PV} \cdot A \cdot \Phi \cdot \eta, \tag{11}$$

The radiation heat losses trough both front and back surfaces are calculated using the following expressions, respectively [8].

$$q_{rad-front} = \sigma \cdot F_{mfsky} \cdot \epsilon_{front} \cdot A \cdot (T_{fs}^4 - T_{sky}^4) + \sigma \cdot F_{mfgr} \cdot \epsilon_{front} \cdot A \cdot (T_{fs}^4 - T_{ground}^4). \tag{12}$$

$$q_{rad-back} = \sigma \cdot F_{mbsky} \cdot \epsilon_{back} \cdot A \cdot (T_{bs}^4 - T_{sky}^4) + \sigma \cdot F_{mfgr} \cdot \epsilon_{back} \cdot A \cdot (T_{bs}^4 - T_{ground}^4). \tag{13}$$

The view factors are calculated using the expressions given in Section 4.3.3 (point number 10). The sky temperature is, $T_{sky} = (T_{ambien} - \delta T)$ for clear sky condition where $\delta T = 20K$, $T_{sky} = T_{ambient}$ for overcast condition [29]. The ground temperature is assumed to be equal to the ambient temperature.

Both free and forced convection mechanisms are considered in creating this thermal model. Their overall effect is calculated by combining their effect using Equation T.1.2 from Table 1. For both mechanisms, we treat the front and back surface individually because the properties of the film layer at the boundary of each one are different. The free convection heat loss is determined using Equations (14) to (18), in which the subscript x refers to the front (f) or back (b) surface; therefore, during implementation, the equation has to be rewritten for each surface.

$$Gr_x = \frac{g \cdot \rho_{air,x}^2 \cdot \cos(\theta) \cdot \beta_x \cdot \Delta T \cdot L_c^3}{\mu_{air,x}^2}, \tag{14}$$

$$Ra_x = Gr_x \cdot Pr_x, \tag{15}$$

$$Nu_{free,f} = 0.27 \cdot Ra_f^{0.25}, \quad (16)$$

$$Nu_{free,b} = 0.54 \cdot Ra_b^{0.25}, \quad (17)$$

$$h_{free,x} = Nu_{free,x} \frac{k_{air,x}}{L_c}, \quad (18)$$

For estimating the forced convection coefficients (for both surfaces), we modify the expressions used by Kayhan [13], given as

$$Re_x = \frac{V_w \cdot L_c \cdot \rho_{air,x}}{\mu_x}, \quad (19)$$

$$h_{forced,x} = \frac{k_{air,x}}{L_c} \cdot (2 + 0.41 \cdot Re_x) \cdot H_x. \quad (20)$$

The introduced modification can be seen in Equation (20) where we added a novel coefficient (H), which is defined as the forced convection adjustment coefficient for both front and back surfaces. This coefficient modulates the relationship between the tilt angle and the wind effect on the amount of heat loss by forced convection. This coefficient is calculated as

$$H_f = (1 + \cos(\beta_{surface})) / m, \quad (21)$$

$$H_b = (1 - \cos(\beta_{surface})) / m, \quad (22)$$

where m is an empirical factor estimated with the help of measurement data. The following points explain the fundamental concept behind the coefficient H by considering PV module mounted with different tilt angles and assuming that the value of m is equal to 2.

- 0° tilt angle:
 - The front surface will undergo a maximum effect of the wind that will sweep the hot air away. This fact is ensured by Equation (21), which will be evaluated to 1. That is, the expression used for calculating the heat loss by forced convection will not be disturbed by the tilt angle.
 - For a typical PV system, there are two facts: First, the system is consisting of many PV modules with a defined density. Second, PV modules are mounted close to the ground in case of flat and small tilt angles. Therefore, the wind will have no considerable effect on the back surface of the PV module. Equation (22) will be evaluated to zero for a flat surface; that is, the forced convection heat loss from the back surface will be neglected in this case.
- 60° tilt angle:
 - This implies that the wind will face resistance from the front surface of the PV module compared to the case of flat mounting. Therefore, reducing the ability to sweep out the hot air away from the surface. Equation (21) will be evaluated to 0.75. That is, the tilt angle will be a reason for reducing the amount of heat loss by forced convection.
 - The lower surface will be facing the wind, which was not the case for a flat-mounted module. Equation (22) will be evaluated to 0.25. Thus, heat loss by forced convection is much higher compared to flat or small tilt angles. However, it is still lower compared to the front surface.
- 90° tilt angle: Both front and back surfaces will be directly facing the air flow. Therefore, neglecting the wind direction for its minor effect compared to its speed [25,26], the wind will equally act on both surfaces. Both Equations (21) and (22) will be evaluated to 0.5.

Therefore, we consider that the PV module tilt angle will control the amount of heat losses from both surfaces. For tilt angles between 0° and 90°, the front surface heat loss by forced convection is higher compared to the back surface. Increasing the tilt angle (within this range) produces lower forced convection heat loss from the front surface and higher from the back surface.

We claim that m is a factor that affects the relationship between the tilt angle and the heat loss by forced convection by involving other installation parameters. These parameters include the PV modules installation density, the elevation from the ground and the thickness at the module edges at which the wind speed drops to zero. From experience, we found that this empirical factor has a value in the range between 1.5 and 2. Therefore, in this paper, we consider scanning this range with a specific resolution and running the model for each value. By increasing the resolution more, the value of m can be determined more accurately. Based on experience, We consider 0.1 as a resolution value considering a trade-off between the computational cost and accuracy. Therefore, we consider running the thermal model six times after which we decide what is the best value for m (by monitoring the error indication parameters) to be fixed for the module under investigation.

Once we have the value of the empirical factor m , we substitute it in Equations (21) and (22) to determine the forced convection adjustment coefficient for the front and back surface, respectively. For each surface, the overall convection coefficient and the corresponding rate of convection thermal energy losses can be calculated using the Equations T 1.2 from Tables 1 and 6.

Table 6. PV modules technical specifications, physical and installation parameters.

Parameter	Polycrystalline	Amorphous
Module dimensions	1645 × 990 × 50 mm	350 × 300 × 25 mm
Front side	Tempered glass	Tempered glass
PV layer	Polycrystalline Silicon	Amorphous Silicon
Encapsulating material	EVA	EVA
Back side	tedlar	tedlar
efficiency	12.64%	11.5%
Tilt angle	20	47
α_{fg}	0.04	0.04
α_{pV}	0.93	0.93
τ_{pV}	0.94	0.94
ϵ_{front}	0.91	0.91
ϵ_{back}	0.85	0.85

The proposed model also considers the following points.

- The characteristics length L_c is considered as the longest dimension of the PV module.
- The model operates to determine the PV electronic junction temperature. This temperature is correlated to the front and back surfaces employing temperature differences. Each temperature difference is defined as the total heat losses from the corresponding surface multiplied by the thermal resistivity of half of the PV structure (the volume between the half of the semiconductor layer plane and the corresponding surface plane), as shown in Figure 2.
- The Newton–Raphson iterative method is employed to solve the model and calculate the output PV layer, front surface and back surface temperatures.
- Therefore, with each iteration, the following two equations are evaluated to calculate the front and back surface temperatures, respectively,

$$\Delta T_f = q_{front-total} \cdot R_f \quad (23)$$

$$\Delta T_b = q_{back-total} \cdot R_b \quad (24)$$

where $q_{front-total}$ and $q_{back-total}$ are the total thermal losses from the front and back side of the PV module, respectively. R_f , and R_b are the thermal resistivity of the PV module, between the front and back surfaces and the active layer, respectively.

6. Results and Discussion

This model has been validated using a polycrystalline and an amorphous PV module. The validation data of the polycrystalline module has been taken from a reference [9]. Our measurement system has been used to collect the amorphous module validation data. This measurement system provides data such as PV module back surface temperature, full I–V curve, global solar irradiance, ambient temperature and wind speed. The global irradiance was measured by Delta Ohm LP RAD 03 piranometer that detect solar irradiance ranging from 0 to 2000 W/m². The temperature of the PV module is recorded using a circuit board attached to the back side of the module with a thermal conductive adhesive. The circuit includes a temperature sensor IC (MAX6603ATB+T). The accuracy of the circuit is ± 0.8 °C at +25 °C. The ambient temperature is measured using PT100 resistance thermometers. Wind speed data is taken from a wind turbine FD2.5-300 which is capable of measuring range of 0 to 60 m/s with an accuracy of ± 0.3 m/s.

Table 6 shows the technical specifications and physical parameters of both modules, which are required for running the model.

To verify the model, we use measurement data including irradiances, ambient temperatures and wind speed that have been recorded for two different full days for each module. For the amorphous module, the two days were the 5th and the 11th of October. For the polycrystalline module, the two days were the 3rd and the 26th of July. The main difference between the two days of each module is the wind speed. The average wind speed is 6.14 m/s on the 26th and 2.16 m/s on the 3rd of July, while it is 2.05 m/s on the 5th and 0.77 m/s on the 11th of October. As mentioned in Table 6, each module has a different tilt angle. Based on our experience, we claim that the module tilt angle has a significant effect on the value of the thermal energy losses by forced convection. As described in the model introduced in Section 5, we introduced a forced convection adjustment coefficient (H) and its empirical factor (m). In this regard, we report that the value of m typically takes a value between 1.5 and 2. We calculate this factor by scanning its range and running the model with a step of 0.1.

For evaluating the proposed model and validating the results we use two error indication parameters: one is the root mean square error ($RMSE$) and the other is the correlation coefficient (r). These parameters are used, as shown in Table 7, to compare the module's back surface temperature for each day (entire day measurement) of the two modules with the estimated values using the proposed model for different values of m .

Table 7. Error quantifying parameters corresponding different m values.

m	Polycrystalline				Amorphous			
	3rd July		26th July		5th July		11th July	
	$RMSE$ [°C]	r	$RMSE$ [°C]	r	$RMSE$ [°C]	r	$RMSE$ [°C]	r
1.3	1.724	0.997	3.099	0.964	1.455	0.965	2.089	0.966
1.4	1.329	0.996	1.740	0.989	1.312	0.971	1.906	0.969
1.5	1.051	0.997	1.090	0.994	1.208	0.976	1.832	0.970
1.6	0.927	0.997	0.937	0.997	1.140	0.978	1.707	0.972
1.7	0.964	0.996	1.228	0.997	1.106	0.980	1.646	0.973
1.8	1.126	0.996	1.558	0.997	1.101	0.980	1.577	0.975
1.9	1.315	0.996	1.891	0.996	1.119	0.979	1.585	0.975
2.0	1.534	0.996	2.216	0.996	1.310	0.971	1.606	0.974

Based on the results shown in Table 7, we chose a value of $m = 1.6$ for the polycrystalline module and $m = 1.8$ for the amorphous module to be used in this study, as these values give the best results. Figure 3 shows both the measured and the estimated PV module back surface temperature for the polycrystalline module, for the two investigated days: 3rd and 26th of July. Each curve includes 120 points as a result of recording the temperatures every 5 min between 9 am and 7 pm.

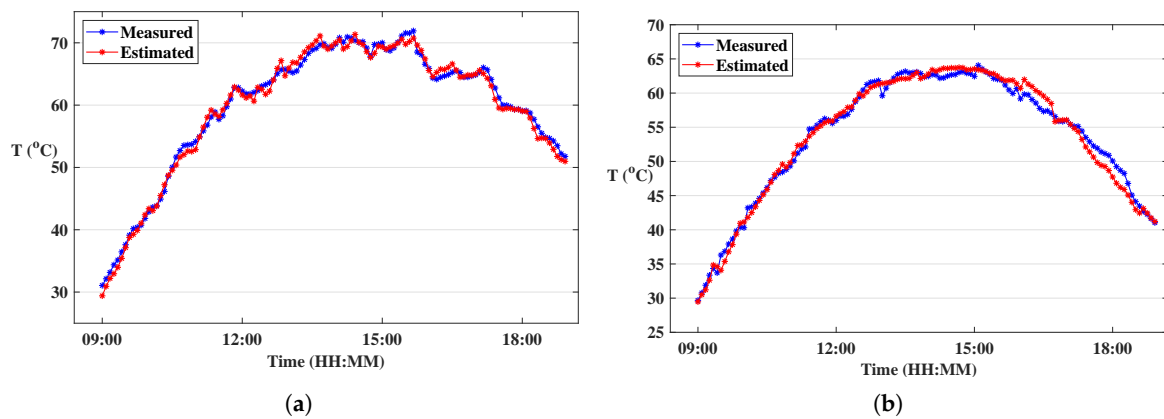


Figure 3. Measured and estimated polycrystalline module backside temperature. (a) 3rd July. (b) 26th July.

Figure 4 shows both the measured and the estimated PV module back surface temperature for the amorphous module, for the two investigated days, 5th of October (49 points between 9 am and 1 pm) and 11th of October (71 points between 9 am and 3 pm).

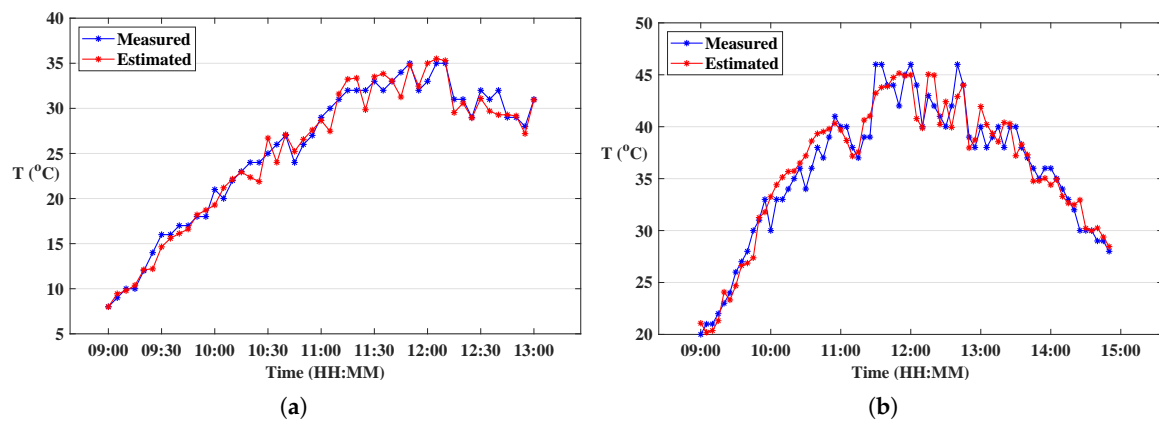


Figure 4. Measured and estimated amorphous module backside temperature. (a) 5th October. (b) 11th October.

Figure 5 shows the absolute value of the temperature difference between the measured and estimated values of the back surface temperature using the proposed model for both modules.

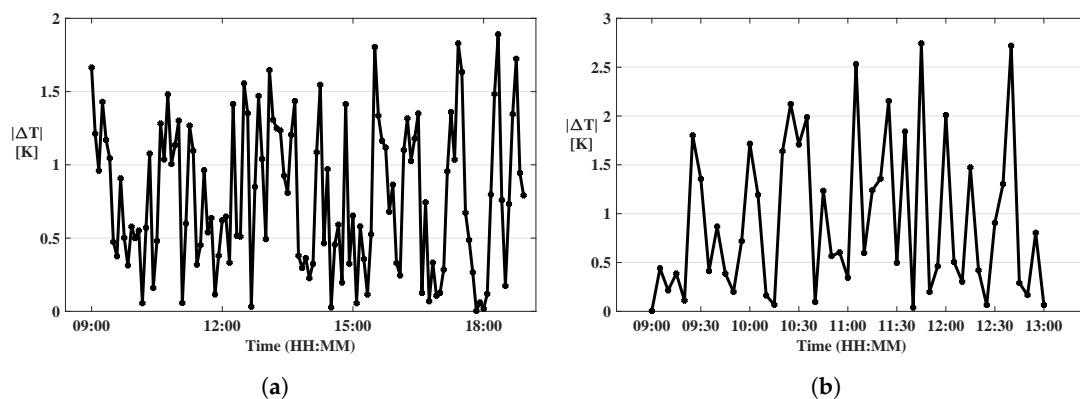


Figure 5. Absolute values of the temperature difference between the measured and the estimated values. (a) Polycrystalline 3rd October. (b) Amorphous 5th October.

Figure 6 shows the relationship between the junction temperature and both surfaces temperatures. It illustrates how these temperature differences are changing with the time of day. Therefore, it will provide a clear picture of the temperature profile across the PV module. The temperature difference to the front surface (ΔT_f) is ranging from 0.7 to 2.5, with an average value of 1.86 °C. The temperature difference to the back surface is between 1.67 and 0.22 with 0.96 °C as an average value.

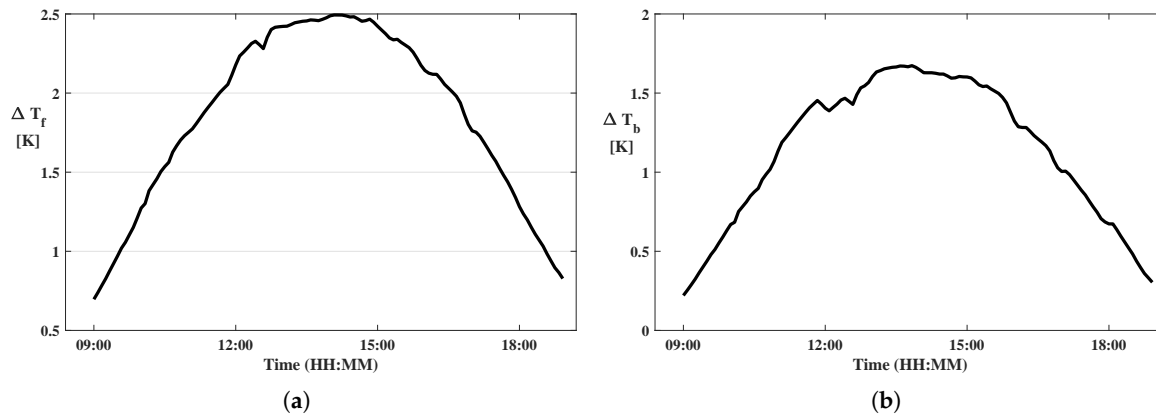


Figure 6. Temperature difference between the electronic junction and the polycrystalline module (measurements used for 3rd July) front and back surfaces. (a) Difference to the front surface. (b) Difference to the back surface.

Figure 7 highlight the importance of the novel coefficient and the consideration of the tilt angle in the forced convection, introduced in this paper. The same figure also shows the effect of neglecting the wind in the thermal model. Figure 7a compares the measured back surface temperature (blue colour) to the estimated temperature with the coefficient H (red colour), without the coefficient H (black colour), and without wind effect (green colour), for the polycrystalline module (measurements used for 3rd July). Figure 7b shows the absolute error to compare different situations.

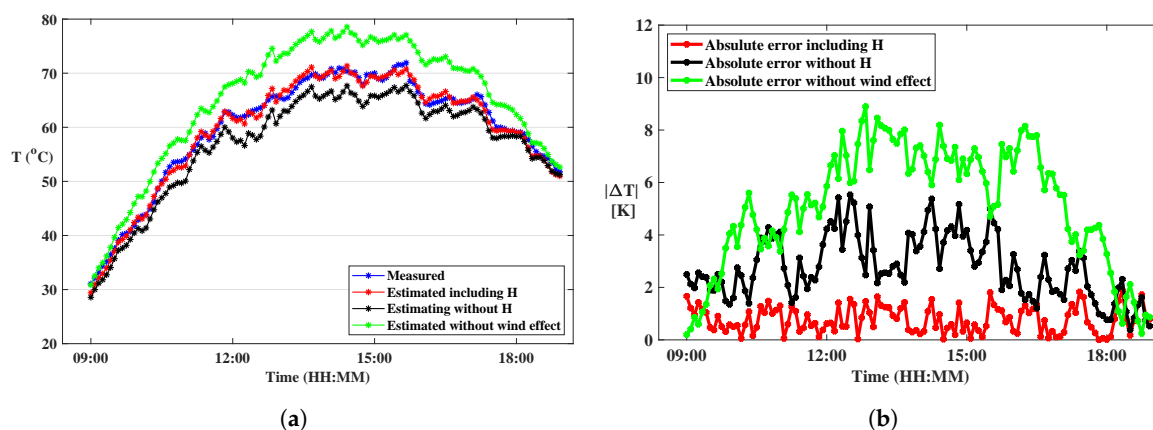


Figure 7. Evaluating the effect of including H in the PV thermal model (the model applied for the polycrystalline module, measurements used for 3rd July). (a) Compares back surface temperatures. (b) Compares the absolute error.

According to the results shown above, we summarise the discussion with the following points.

- One of the focus points of the proposed model is the special dependence of forced convection mechanism on the module tilt angle.
- Two modules made with different technologies and mounted with different tilt angles were used to validate the proposed model. A forced convection adjustment coefficient (H) has been

considered for this purpose, which includes an empirical factor (m). We calculate this factor by scanning its range as discussed above.

- For each module, the model has been validated using measurements of two days with different average wind speeds.
- Table 7 shows the proposed model’s ability to estimate the temperature with high accuracy characterised by the two error quantifying parameters, namely, $RMSE$ and r . It is worth mentioning that the model provides low error rate for all values of m . However, the highest accuracy is realised at an optimum value of the factor m .
- From Figures 3 and 4, we see that the model results represented by the backside estimated temperature followed the experimentally measured values for PV modules of different technologies, different tilt angles and different wind speeds by measurements collected on two different days for each module.
- Figure 5 shows the absolute difference between the measured and the estimated values using the proposed model for both modules. Figure 5a shows that this value is always below 2 °C, with an average value of 0.78 °C for the polycrystalline module (measurements used for 3rd July). Figure 5b shows similar results for the amorphous module.
- Figure 7b shows the substitutional effect of the coefficient H on the thermal model, enabling accurate temperature estimation for the PV modules. The same figure also shows that large error is produced in case of neglecting the wind effect (neglecting the forced convection heat transfer mechanism).
- Figure 6 shows that the temperature difference between the PV electronic junction plane and both surfaces reach their maximum values around the midday time at which both ambient and electronic junction temperature are at their maximum values. This happens because the ambient temperature is higher at midday; thus, the temperature difference between the module surface and the ambient is smaller that will reduce the rate of the heat loss from the module to the surrounding.
- Table 8 shows the achieved accuracy of the proposed model using the two modules under different environmental conditions, represented by two introduced error quantifying parameters $RMSE$ and r .

Table 8. Thermal model accuracy achieved for the two modules.

PV Module	Date	$RMSE$ [°C]	r
Polycrystalline-module	3rd July	0.927	0.997
	26th July	0.937	0.997
Amorphous-module	5th October	1.101	0.980
	11th October	1.577	0.975

- For the same module, typically, $\Delta T_f > \Delta T_b$. Therefore, the top surface temperature is slightly lower than the backside temperature due to, relatively, more effective heat transfer mechanisms.

The rest of this section is dedicated to highlighting the scientific improvement that has been introduced in this work. We made a comparison between the proposed model and the results reported by different thermal models from the recent and most accurate literature using various error quantifying parameters. In this comparison, we will refer to the best results reported by the references and compare it to our model using the measurement recorded on the 3rd of July for the polycrystalline module.

- Several thermal models found in the literature use the root mean square error ($RMSE$) as an error quantifying parameter to validate the results. The models presented in [16,18,23,28,31,32,38,42,45,46] have reported $RMSE$ values ranging between 4.9 and 1.1 °C. However, in our presented model we report a value of 0.927 °C.

- The correlation coefficient (r) is another parameter used in the literature. Thermal model presented in [16,23] reported $r = 0.98$, and 0.95 , respectively. In our thermal model, we calculate a correlation coefficient of 0.997 .
- The authors of [40] used the relative error to validate their proposed thermal model by comparison with other models. They reported an average deviation of 2.7% . Calculating the same error indication parameter using our proposed model gives 1.26% .

7. Conclusions

In this paper, we introduced a novel thermal model to predict the PV electronic junction, front surface and back surface temperatures. The model has been verified using on-site measurement for two modules made with two different technology and mounted with different tilt angles. The measurements have been recorded for each module for two different days in which the average wind speed is the main difference. A novel concept has been introduced to consider the module tilt angle effect on the amount of heat loss by forced convection. The result presented in Table 8 shows that the model is able to estimate the PV module temperature with high accuracy represented by $RMSE = 0.927$ °C and $r = 0.997$ as the best results for both modules under the considered environmental conditions. From the same table, calculating the average of these parameters give $RMSE = 1.1$ °C and $r = 0.987$, which are comparable, but slightly better compared to the best results review from the literature. During the model validation phase, we found that obtaining a high level of accuracy is only possible by including a novel forced convection adjustment coefficient (H). Using the same proposed model without this coefficient gives $RMSE = 3.02$ °C when applying the model to estimate the junction temperature of the polycrystalline module (3rd July). The back surface temperature absolute differences between the measured and the estimated values have been calculated for both modules, which give an average value below 1 °C for both studied modules, considering the two days measurements for both. The following points summarise this work's conclusion.

- Based on the introduced and discussed results, the proposed model shows the ability to estimate the PV module temperature of different technologies, mounting tilt angles and environmental conditions.
- Based on the proceeding discussion and the information delivered in Figure 7, it is evident that the coefficient H introduces a significant improvement to the result accuracy of PV thermal modelling.
- We have also concluded that wind is an essential parameter to be considered in PV thermal modelling. Running our model with neglecting the wind effect raises the $RMSE$ from 0.927 °C to 5.62 °C.
- The presented work proves that considering the static approach in this model provides excellent accuracy level of PV module temperature estimation even with a resolution of 5 min for the polycrystalline module.
- The electronic junction temperature as well as both front and back surface temperatures delivered by the model could be used in studying the PV module temperature profile, mechanical properties and lifetime.

It worth highlighting at this point that the novelty of the proposed paper is realized by introducing the new forced convection adjustment coefficient, and by reviewing the most often used existing expressions for calculating the different forms of the PV module heat losses and the related parameters and finding the proper combination of these expressions to be employed in the presented model.

Author Contributions: Individual author contributions are as follows: Conceptualization, A.K.A and G.B.; software, A.K.A. and G.B.; validation, A.K.A., G.B. and B.P.; writing—original draft preparation, A.K.A.; writing—review and editing, A.K.A., G.B. and B.P. All authors have read and agreed to the published version of the manuscript.

Funding: The research reported in this paper was supported by the BME Nanotechnology and Materials Science TKP2020 IE grant of NKFIH Hungary (BME IE-NAT TKP2020), by the Stipendium Hungaricum Scholarship

Programme, the grant EFOP-3.6.1-16-2016-00014 and by the Science Excellence Program at BME under the grant agreement NKFIH-849-8/2019 of the Hungarian National Research, Development and Innovation Office.

Conflicts of Interest: The authors declare no conflicts of interest.

List of Symbols and Abbreviations

HBE	Heat balance equation
FF	Fill factor (-)
I_{sc}	Short circuit current (A)
V_{oc}	Open circuit voltage (V)
I_m	Current at the maximum power point (A)
V_m	Voltage at the maximum power point (V)
T	Temperature (K)
C	Thermal capacitance (J K ⁻¹)
C_{module}	Total module thermal capacitance (J K ⁻¹)
d	Layer thickness (m)
c	Specific heat (J kg ⁻¹ K ⁻¹)
cp_{air}	Specific heat at constant pressure of air (J kg ⁻¹ K ⁻¹)
h_c	Convection heat transfer coefficients (W m ⁻² K ⁻¹)
q	Heat flux (W m ⁻²)
q_1	Heat flux absorbed by the tempered glass layer (W m ⁻²)
q_2	Heat flux absorbed by the semiconductor layer (W m ⁻²)
q_{conv}	Convection heat flux (W m ⁻²)
q_{rad}	Radiation heat flux (W m ⁻²)
$h_{c,forced}$	Forced convection coefficient (W m ⁻² K ⁻¹)
$h_{c,free}$	Free convection coefficient (W m ⁻² K ⁻¹)
L_c	PV module characteristics length (m)
ΔT	Temperature difference between the PV module surface and the ambient temperatures (K)
ΔT_f	Temperature difference between the PV module junction and its front side surface (K)
ΔT_b	Temperature difference between the PV module junction and its back side surface (K)
δT	Constant value (K)
T_f	The average between the surface and ambient temperatures (K)
Gr	Grashof number (-)
Nu	Nusselt number (-)
Nu_{forced}	Nusselt number of the forced convection (-)
Nu_{free}	Nusselt number of the free convection (-)
Ra	Rayleigh number (-)
Pr	Prandtl number (-)
Re	Reynolds number (-)
k_{air}	Thermal conductivity of air (W m ⁻¹ K ⁻¹)
W	Module width (m)
S	Module perimeter (m)
A	Module area (m ²)
F	View factor (-)
H	Forced convection adjustment coefficient (-) or module length (m)
m	Empirical factor of the forced convection to the tilt angle and wind relationship (-)
RMSE	Root mean square error (°C)
r	Correlation coefficient (-)

Greek letters

α	Absorptivity (-)
α_{fg}	Absorptivity of the glass layer (-)
α_{PV}	Absorptivity of the semiconductor layer (-)
Φ	Total received irradiance (W/m^2)
η	Efficiency (-)
τ	Transmittance (-)
τ_{fg}	Transmittance of the glass layer (-)
ρ	Density (kg m^{-3})
β	Module tilt angle ($^\circ$) or air thermal expansion coefficient (K^{-1})
θ	Angle of the module to the vertical axis ($^\circ$)
μ_{air}	Dynamic viscosity of air ($\text{kg m}^{-1} \text{s}^{-1}$)
v_w	Wind speed (m s^{-1})
σ	Stefan–Boltzmann constant ($\text{W m}^{-2} \text{K}^{-4}$)
ϵ	Emissivity (-)

References

1. Motiei, P.; Yaghoubi, M.; GoshtashbiRad, E.; Vadiee, A. Two-dimensional unsteady state performance analysis of a hybrid photovoltaic-thermoelectric generator. *Renew. Energy* **2018**, *119*, 551–565. [[CrossRef](#)]
2. Chopde, A.; Magare, D.; Patil, M.; Gupta, R.; Sastry, O.S. Parameter extraction for dynamic PV thermal model using particle swarm optimisation. *Appl. Therm. Eng.* **2016**, *100*, 508–517. [[CrossRef](#)]
3. Kant, K.; Shukla, A.; Sharma, A.; Biwole, P.H. Thermal response of poly-crystalline silicon photovoltaic panels: Numerical simulation and experimental study. *Sol. Energy* **2016**, *134*, 147–155. [[CrossRef](#)]
4. Aly, S.P.; Ahzi, S.; Barth, N.; Figgis, B.W. Two-dimensional finite difference-based model for coupled irradiation and heat transfer in photovoltaic modules. *Sol. Energy Mater. Sol. Cells* **2018**, *180*, 289–302. [[CrossRef](#)]
5. Armstrong, S.; Hurley, W.G. A thermal model for photovoltaic panels under varying atmospheric conditions. *Appl. Therm. Eng.* **2010**, *30*, 1488–1495. [[CrossRef](#)]
6. Aly, S.P.; Ahzi, S.; Barth, N.; Abdallah, A. Using energy balance method to study the thermal behavior of PV panels under time-varying field conditions. *Energy Convers. Manag.* **2018**, *175*, 246–262. [[CrossRef](#)]
7. Zhao, B.; Chen, W.; Hu, J.; Qiu, Z.; Qu, Y.; Ge, B. A thermal model for amorphous silicon photovoltaic integrated in ETFE cushion roofs. *Energy Convers. Manag.* **2015**, *100*, 440–448. [[CrossRef](#)]
8. Balog, R.S.; Kuai, Y.; Uhrhan, G. A photovoltaic module thermal model using observed insolation and meteorological data to support a long life, highly reliable module-integrated inverter design by predicting expected operating temperature. In Proceedings of the 2009 IEEE Energy Conversion Congress and Exposition (ECCE 2009), San Jose, CA, USA, 20–24 September 2009; pp. 3343–3349. [[CrossRef](#)]
9. Santiago, I.; Trillo-Montero, D.; Moreno-Garcia, I.; Pallarés-López, V.; Luna-Rodríguez, J. Modeling of photovoltaic cell temperature losses: A review and a practice case in South Spain. *Renew. Sustain. Energy Rev.* **2018**, *90*, 70–89. [[CrossRef](#)]
10. Verma, V.; Kane, A.; Singh, B. Complementary performance enhancement of PV energy system through thermoelectric generation. *Renew. Sustain. Energy Rev.* **2016**, *58*, 1017–1026. [[CrossRef](#)]
11. Kosyachenko, L.A. *Solar Cells—New Approaches and Reviews*; IntechOpen: Rijeka, Croatia, 2015. [[CrossRef](#)]
12. Jacques, S.; Caldeira, A.; Ren, Z.; Schellmanns, A.; Batut, N. Impact of the cell temperature on the energy efficiency of a single glass PV module: Thermal modeling in steady-state and validation by experimental data. In Proceedings of the International Conference on Renewable Energies and Power Quality (ICREPPQ'13), Bilbao, Spain, 20–22 March 2013.
13. Kayhan, Ö. A thermal model to investigate the power output of solar array for stratospheric balloons in real environment. *Appl. Therm. Eng.* **2018**, *139*, 113–120. [[CrossRef](#)]
14. Solanki, C.S.; Singh, H.K. *Anti-Reflection and Light Trapping in c-Si Solar Cells*; Green Energy and Technology; Springer: Singapore, 2017; pp. 17–41. [[CrossRef](#)]
15. Mattei, M.; Notton, G.; Cristofari, C.; Muselli, M.; Poggi, P. Calculation of the polycrystalline PV module temperature using a simple method of energy balance. *Renew. Energy* **2006**, *31*, 553–567. [[CrossRef](#)]

16. Akhsassi, M.; El Fathi, A.; Erraissi, N.; Aarich, N.; Bennouna, A.; Raoufi, M.; Outzourhit, A. Experimental investigation and modeling of the thermal behavior of a solar PV module. *Sol. Energy Mater. Sol. Cells* **2018**, *180*, 271–279. [[CrossRef](#)]
17. Schwingshackl, C.; Petitta, M.; Wagner, J.E.; Belluardo, G.; Moser, D.; Castelli, M.; Zebisch, M.; Tetzlaff, A. Wind Effect on PV Module Temperature: Analysis of Different Techniques for an Accurate Estimation. *Energy Procedia* **2013**, *40*, 77–86. [[CrossRef](#)]
18. Notton, G.; Cristofari, C.; Mattei, M.; Poggi, P. Modelling of a double-glass photovoltaic module using finite differences. *Appl. Therm. Eng.* **2005**, *25*, 2854–2877. [[CrossRef](#)]
19. Guerriero, P.; Codecasa, L.; D’Alessandro, V.; Daliento, S. Dynamic electro-thermal modeling of solar cells and modules. *Sol. Energy* **2019**, *179*, 326–334. [[CrossRef](#)]
20. Sahli, M.; Correia, J.P.M.; Ahzi, S.; Touchal, S. Multi-physics modeling and simulation of heat and electrical yield generation in photovoltaics. *Sol. Energy Mater. Sol. Cells* **2018**, *180*, 358–372. [[CrossRef](#)]
21. Weiss, L.; Amara, M.; Ménézo, C. Impact of radiative-heat transfer on photovoltaic module temperature. *Prog. Photovolt. Res. Appl.* **2016**, *24*, 12–27. [[CrossRef](#)]
22. Kaplani, E.; Kaplanis, S. Thermal modelling and experimental assessment of the dependence of PV module temperature on wind velocity and direction, module orientation and inclination. *Sol. Energy* **2014**, *107*, 443–460. [[CrossRef](#)]
23. Usama Siddiqui, M.; Arif, A.F.M.; Kelley, L.; Dubowsky, S. Three-dimensional thermal modeling of a photovoltaic module under varying conditions. *Sol. Energy* **2012**, *86*, 2620–2631. [[CrossRef](#)]
24. Vogt, M.R.; Holst, H.; Winter, M.; Brendel, R.; Altermatt, P.P. Numerical Modeling of c-Si PV Modules by Coupling the Semiconductor with the Thermal Conduction, Convection and Radiation Equations. *Energy Procedia* **2015**, *77*, 215–224. [[CrossRef](#)]
25. Kaldellis, J.K.; Kapsali, M.; Kavadias, K.A. Temperature and wind speed impact on the efficiency of PV installations. Experience obtained from outdoor measurements in Greece. *Renew. Energy* **2014**, *66*, 612–624. [[CrossRef](#)]
26. Gu, X.; Yu, X.; Guo, K.; Chen, L.; Wang, D.; Yang, D. Seed-assisted cast quasi-single crystalline silicon for photovoltaic application: Towards high efficiency and low cost silicon solar cells. *Sol. Energy Mater. Sol. Cells* **2012**, *101*, 95–101. [[CrossRef](#)]
27. Skoplaki, E.; Palyvos, J.A. Operating temperature of photovoltaic modules: A survey of pertinent correlations. *Renew. Energy* **2009**, *34*, 23–29. [[CrossRef](#)]
28. Muzathik, A.M. Photovoltaic Modules Operating Temperature Estimation Using a Simple Correlation. *Int. J. Energy Eng.* **2014**, *4*, 151–158.
29. Jones, A.; Underwood, C. A thermal model for photovoltaic systems. *Sol. Energy* **2001**, *70*, 349–359. [[CrossRef](#)]
30. Torres-Lobera, D.; Valkealahti, S. Inclusive dynamic thermal and electric simulation model of solar PV systems under varying atmospheric conditions. *Sol. Energy* **2014**, *105*, 632–647. [[CrossRef](#)]
31. Torres Lobera, D.; Valkealahti, S. Dynamic thermal model of solar PV systems under varying climatic conditions. *Sol. Energy* **2013**, *93*, 183–194. [[CrossRef](#)]
32. Tsai, H.F.; Tsai, H.L. Implementation and verification of integrated thermal and electrical models for commercial PV modules. *Sol. Energy* **2012**, *86*, 654–665. [[CrossRef](#)]
33. Kurz, D.; Nawrowski, R. Thermal time constant of PV roof tiles working under different conditions. *Appl. Sci.* **2019**, *9*. [[CrossRef](#)]
34. Sánchez Barroso, J.C.; Barth, N.; Correia, J.P.M.; Ahzi, S.; Khaleel, M.A. A computational analysis of coupled thermal and electrical behavior of PV panels. *Sol. Energy Mater. Sol. Cells* **2016**, *148*, 73–86. [[CrossRef](#)]
35. Faiman, D. Assessing the outdoor operating temperature of photovoltaic modules. *Prog. Photovolt. Res. Appl.* **2008**, *16*, 307–315. [[CrossRef](#)]
36. Franghiadakis, Y.; Tzanetakakis, P. Explicit empirical relation for the monthly average cell-temperature performance ratio of photovoltaic arrays. *Prog. Photovolt. Res. Appl.* **2006**, *14*, 541–551. [[CrossRef](#)]
37. Ventura, C.; Tina, G.M. Utility scale photovoltaic plant indices and models for on-line monitoring and fault detection purposes. *Electr. Power Syst. Res.* **2016**, *136*, 43–56. [[CrossRef](#)]
38. Veldhuis, A.J.; Nobre, A.M.; Peters, I.M.; Reindl, T.; Ruther, R.; Reinders, A.H.M.E. An Empirical Model for Rack-Mounted PV Module Temperatures for Southeast Asian Locations Evaluated for Minute Time Scales. *IEEE J. Photovolt.* **2015**, *5*, 774–782. [[CrossRef](#)]

39. Barth, N.; Al Otaibi, Z.S.; Ahzi, S. Irradiance, thermal and electrical coupled modeling of photovoltaic panels with long-term simulation periods under service in harsh desert conditions. *J. Comput. Sci.* **2018**, *27*, 118–129. [[CrossRef](#)]
40. Gu, W.; Ma, T.; Shen, L.; Li, M.; Zhang, Y.; Zhang, W. Coupled electrical-thermal modelling of photovoltaic modules under dynamic conditions. *Energy* **2019**, *188*, 116043. [[CrossRef](#)]
41. Migliorini, L.; Molinaroli, L.; Simonetti, R.; Manzolini, G. Development and experimental validation of a comprehensive thermoelectric dynamic model of photovoltaic modules. *Sol. Energy* **2017**, *144*, 489–501. [[CrossRef](#)]
42. Palacio Vega, M.A.; González López, O.M.; Martínez Guarín, A.R.; Gómez Vásquez, R.D.; Bula, A.; Mendoza Fandiño, J.M. Estimation of the Surface Temperature of a Photovoltaic Panel Through a Radiation-Natural Convection Heat Transfer Model in Matlab Simulink. In Proceedings of the ASME 2016 International Mechanical Engineering Congress and Exposition, Volume 8: Heat Transfer and Thermal Engineering, Phoenix, AZ, USA, 11–17 November 2016; American Society of Mechanical Engineers: Phoenix, AZ, USA, 2017; doi:10.1115/IMECE2016-66769. [[CrossRef](#)]
43. Cengel, Y. *Heat and Mass Transfer: Fundamentals and Applications*; McGraw-Hill Higher Education: New York, NY, USA, 2014.
44. Sartori, E. Convection coefficient equations for forced air flow over flat surfaces. *Sol. Energy* **2006**, *80*, 1063–1071. [[CrossRef](#)]
45. King, D.L.; Kratochvil, J.A.; Boyson, W.E. *Photovoltaic Array Performance Model*; United States Department of Energy: Livermore, CA, USA, 2004.
46. Barykina, E.; Hammer, A. Modeling of photovoltaic module temperature using Faiman model: Sensitivity analysis for different climates. *Sol. Energy* **2017**, *146*, 401–416. [[CrossRef](#)]



© 2020 by the authors. Licensee MDPI, Basel, Switzerland. This article is an open access article distributed under the terms and conditions of the Creative Commons Attribution (CC BY) license (<http://creativecommons.org/licenses/by/4.0/>).